toxics

MDPI

Article

Migration Behavior of Technetium-99 in Granite, Clay Rock, and Shale: Insights into Anionic Exclusion Effects

Yunfeng Shi, Song Yang, Wenjie Chen, Aiming Zhang, Zhou Li, Longjiang Wang * and Bing Lian *

Department of Nuclear Environmental Science, China Institute for Radiation Protection (CIRP), Taiyuan 030006, China; shiyunfeng@cirp.org.cn (Y.S.)

* Correspondence: wanglongjiang@cirp.org.cn (L.W.); lianbing@cirp.org.cn (B.L.); Tel.: +86-15103418769 (L.W.)

Abstract

One of the key tasks in the geological disposal of radioactive waste is to investigate the blocking ability of different host rocks on nuclide migration in the disposal site. This study conducted experimental and numerical methods to the adsorption, diffusion, and advection–dispersion behavior of ^{99}Tc in three types of rocks: granite, clay rock, and mudstone shale, with a focus on the influence of anion exclusion during migration. The research results found that the three types of rocks have no significant adsorption effect on ^{99}Tc, and the anion exclusion during diffusion and advection–dispersion processes can block small "channels", causing some nuclide migration to lag, and accelerate the nuclide migration rate in larger "channels". In addition, parameters characterizing the size of anion exclusion in different migration behaviors, such as effective diffusion coefficient (*De*) and immobile liquid region porosity (θ_{im}), were fitted and obtained.

Keywords: granite; clay rock; mudstone shale; anion exclusion; ^{99}Tc

check for updates

Academic Editors: Luis Alberto Henríquez Hernández and Xiaoxia Lu

Received: 12 August 2025
Revised: 28 August 2025
Accepted: 4 September 2025
Published: 7 September 2025

Citation: Shi, Y.; Yang, S.; Chen, W.; Zhang, A.; Li, Z.; Wang, L.; Lian, B. Migration Behavior of Technetium-99 in Granite, Clay Rock, and Shale: Insights into Anionic Exclusion Effects. *Toxics* **2025**, *13*, 760. https://doi.org/10.3390/toxics13090760

Copyright: © 2025 by the authors. Licensee MDPI, Basel, Switzerland. This article is an open access article distributed under the terms and conditions of the Creative Commons Attribution (CC BY) license (https://creativecommons.org/licenses/by/4.0/).

1. Introduction

Radioactive waste is a unique byproduct generated during the use of atomic energy, and its safe disposal has always been a focal point of public concern. According to the IAEA safety standards, radioactive wastes are categorized into six groups based on their radioactivity levels, ranging from highest to lowest: high-level waste (HLW), intermediate-level waste (ILW), low-level waste (LLW), very low-level waste (VLLW), very short-lived waste (VSLW), and exempt waste (EW) [1]. With the exception of short-lived waste and EW, all other types of waste must undergo various disposal methods, such as near-surface disposal, intermediate-depth disposal, and deep geological repository, for long-term management. The migration of radioactive nuclides from the waste to the surrounding environment must be effectively impeded and isolated through a "multi-barrier system" [2]. Therefore, evaluating the barrier capabilities of different rock types against nuclides is a crucial task in the selection and construction of radioactive waste disposal facilities [3].

Currently, numerous studies have conducted experiments and numerical simulations on the migration of radioactive nuclides through adsorption, diffusion, and convection–dispersion in various types of rocks, yielding a substantial amount of data [4–7]. In recent years, the research focus has transitioned from determining key parameters of nuclide migration behavior to comprehending the primary factors and mechanisms involved in these processes. For instance, Lee investigated the diffusion behavior of Se (IV) in Tamusu clay rocks, emphasizing the impact of compaction density on diffusion behavior [8]. Sun examined the adsorption and diffusion behavior of Se (IV) and Se (VI) in clay rocks,

exploring the influence of different valence states of the same nuclide on their migration behavior [9]. Qi delved into the migration and adsorption behavior of Se (IV) and Sr (II) in granite minerals and fracture fillers, and scrutinized the influence of different chemical forms on the migration behavior of nuclides [10].

In the past, many scholars previously categorized anionic nuclides such as ^{99}Tc (TcO_4^-), ^{129}I (IO_3^-), ^{36}Cl (Cl^-), and ^{3}H (H^+) as non-adsorbed nuclides. Consequently, in numerous hydrogeological experiments, researchers tend to employ anionic elements as tracers to derive geological parameters [11,12], overlooking the "accelerated" migration of nuclides due to anionic exclusion. While some studies have addressed the impact of anionic exclusion on the diffusion and convection–dispersion migration behavior of elements like Cl^- and IO_3^- [13–15], there has been no comprehensive investigation into the effects of anionic exclusion on the adsorption, diffusion, and convection–dispersion of a specific anion nuclide. In 2022, Shi examined the convection–dispersion migration behavior of various iodine ion forms in granite, emphasizing the influence of different chemical forms (I^-/I_3^-) on anionic exclusion [16]. This study offers insights into understanding the "accelerated migration" behavior of anionic nuclides.

^{99}Tc is a significant nuclide found in the waste produced by nuclear power plants, boasting a high fission yield (6.13%) in reactors. Compounds of Tc can display oxidation states ranging from -I to VII, typically existing as TcO_4^- in aqueous solutions [17]. Research on the migration behavior of ^{99}Tc has primarily centered on the impact of changes in nuclide valence states on solubility [18,19] and anionic exclusion [20,21], driven by its unique characteristics of "multiple chemical valence states" and "non-adsorption." The former elucidates how redox conditions in the environment influence the migration of ^{99}Tc in complex settings, aiding in the separation and elimination of ^{99}Tc from multi-nuclide mixed solutions. The latter explores the effects of anionic exclusion on ^{99}Tc migration by comparing its behavior with that of other nuclides in various solid-phase media [22].

Diffusion and advection–dispersion are the primary mechanisms through which radioactive nuclides migrate in the rock medium of disposal sites, influenced by physical and chemical factors. Physical factors pertain to the characteristics of nuclide movement channels within the solid phase medium, defined by parameters like porosity, effective diffusion coefficient, and dispersibility [23]. Chemical factors involve the interaction between nuclides and the surrounding media during migration, particularly in terms of adsorption, with characteristic parameters including distribution coefficient and adsorption rate [24]. The migration of nuclides is concurrently affected by physical and chemical factors. To elucidate the specific role of an influencing factor in nuclide migration, it is typically necessary to initially conduct diffusion and advection–dispersion tests using non-adsorbed nuclides (e.g., HTO) and subsequently introduce designated nuclides to investigate the influencing factors of nuclide migration behavior [25,26].

This study utilized batch experiments [27], diffusion experiments [28], and column experiments [29] to replicate the adsorption, diffusion, and advection–dispersion characteristics of ^{99}Tc in granite, clay rock, and shale. The essential parameters governing the diffusion and advection–dispersion behavior of ^{99}Tc were determined through numerical model fitting [30]. A comparison with the diffusion and advection–dispersion parameters of HTO in the same rock medium facilitated a discussion on the impact of anion repulsion on the migration behavior of ^{99}Tc.

2. Theory of Adsorption, Diffusion, and Advection–Dispersion

2.1. Distribution Coefficient Model

The distribution coefficient is a parameter that characterizes the distribution of nuclides in the solid–liquid phase. According to the IAEA definition, the distribution coefficient is

determined by the ratio of nuclide activity concentration in the solid phase to that in the liquid phase [30]. The expression formula is as follows:

$$K_d = \frac{(c_0 - c_e) \times V}{c_e \times m} \quad (1)$$

where c_0 is the initial activity concentration of nuclides in the liquid phase (Bq/L), c_e is the activity concentration of nuclides in the liquid phase at adsorption equilibrium (Bq/L), V is the total volume of the solution (mL), and M is the mass of the solid phase medium (g).

2.2. Diffusion Model

According to the theory of porous media, rock samples are generalized as isotropic homogeneous porous media, and the diffusion behavior of nuclides in the sample is equivalent to one-dimensional. The diffusion equation is established based on the principle of conservation of mass and the concept of typical unit cells, and the obtained diffusion curve is fitted to the solution of the equation to obtain the diffusion coefficient [31].

$$\frac{\partial C}{\partial t} = \frac{D_a}{R} \frac{\partial^2 C}{\partial x^2} \quad (2)$$

$$D_a = \frac{D_e}{\alpha} \quad (3)$$

$$\alpha = \theta + \rho_b \times k_d \quad (4)$$

$$\theta = 1 - \frac{\rho_b}{\rho_s} \quad (5)$$

The initial conditions and boundary conditions are as follows:
Boundary conditions: $C(x,0) = 0$, $x > 0$
Initial conditions: $C(0,t) = C_0$, $t > 0$

$$C(\infty, t) = 0, \ t \geq 0 \quad (6)$$

where $C(x,t)$ is the concentration distribution of tracer in the vertical direction of the thin slice (Bq/mL), D_e is the effective diffusion coefficient of the tracer in the vertical direction of the thin film (m^2/s), D_a is the apparent diffusion coefficient of the tracer in the vertical direction of the thin film (m^2/s), α is the capacity factor, x is the one-dimensional diffusion distance (cm), t is the diffusion time (d), C_0 is the initial concentration value of each tracer in the source solution tank (Bq/mL), K_d is the adsorption distribution coefficient of the nuclide (mL/g), θ is the total porosity of the porous medium, which is the ratio of the pore volume to the total volume of the medium, ρ_b is the dry density of the solid phase medium (kg/m^3), and ρ_s is the particle density (kg/m^3).

2.3. Advection–Dispersion Model

2.3.1. Equilibrium Transport (E-T)

The one-dimensional equation is as follows [32]:

$$\frac{\partial}{\partial t}(\theta c_r + \rho_b s) = \frac{\partial}{\partial x}\left(\theta D \frac{\partial c_r}{\partial x} - J_w c\right) - \theta \mu_l c_r - \rho_b \mu_s s + \theta r_l(x) + \rho_b r_s(x) \quad (7)$$

where c_r is the volume-averaged or resident concentration of the liquid phase (ML^{-3}); s is the concentration of the adsorbed phase (MM^{-1}); D is the dispersion coefficient (L^2T^{-1}); θ is the volumetric water content (L^3L^{-3}); J_w is the volumetric water flux density (LT^{-1}); ρ_b is the soil bulk density (ML^{-3}); μ_l and μ_s are the first-order decay coefficients for the degradation of the solute in the liquid and adsorbed phases, respectively (T^{-1}); r_l (ML^{-3}

T^{-1}) and r_s ($MM^{-1}\ T^{-1}$) are the zero-order production terms for the liquid and adsorbed phases, respectively; x is the distance (L); and t is the time (T).

The solute adsorption by the solid phase is expressed using a linear isotherm as follows:

$$s = K_d c_r \tag{8}$$

where K_d is an empirical distribution constant ($M^{-1}L^3$). Using (8) and assuming a steady-state flow in a homogeneous soil, (7) may be rewritten as follows:

$$R\frac{\partial c_r}{\partial t} = D\frac{\partial^2 c_r}{\partial x^2} - v\frac{\partial c_r}{\partial x} - \mu c_r + r(x) \tag{9}$$

where $v(=\frac{J_w}{\theta})$ is the average pore-water velocity; R is the retardation factor given by $R = 1 + \frac{\rho_b K_d}{\theta}$; and μ and r are combined first- and zero-order rate coefficients: $\mu = \mu_l + \frac{\rho_b K_d \mu_s}{\theta}$, $r(x) = r_l(x) + \frac{\rho_{br_s}(x)}{\theta}$, respectively.

2.3.2. Two-Region Nonequilibrium Transport (T-N)

A two-region transport model was proposed, and it was assumed that the liquid phase can be partitioned into mobile (flowing) and immobile (stagnant) regions (which are produced by anion exclusion). The solute exchange between the two liquid regions is simulated as a first-order kinetic process. The two-region solute transport model is given by [33].

$$(\theta_m + f\rho_b K_d)\frac{\partial c_m}{\partial t} = \theta_m D_m \frac{\partial^2 c_m}{\partial x^2} - J_w \frac{\partial c_m}{\partial x} - a(c_m - c_{im}) - (\theta_m \mu_{l,m} + f\rho_b K_d \mu_{s,m})c_m + \theta_m r_{l,m}(x) + f\rho_b r_{s,m}(x) \tag{10}$$

$$(\theta_{im} + (1-f)\rho_b K_d)\frac{\partial c_{im}}{\partial t} = a(c_m - c_{im}) - (\theta_{im}\mu_{l,im} + (1-f)\rho_b K_d \mu_{s,im})c_{im} + \theta_{im} r_{l,im}(x) + (1-f)\rho_b r_{s,im}(x) \tag{11}$$

where the subscripts m and im refer to the mobile and immobile liquid regions, respectively; $J_w = v \times \theta = v_m \times \theta_m$ is the volumetric water flux density; f represents the fraction of adsorption sites that equilibrates with the mobile liquid phase; and a is the first-order mass transfer coefficient governing the rate of solute exchange between the mobile and immobile liquid regions. θ is equal to $\theta_m + \theta_{im}$; $\mu_{l,m}$ and $\mu_{l,im}$ are first-order decay coefficients for the mobile and immobile liquid phases, respectively; $\mu_{s,m}$ and $\mu_{s,im}$ are first-order decay coefficients for the mobile and immobile adsorbed phases, respectively; $r_{l,m}$ and $r_{l,im}$ are zero-order production for the mobile and immobile liquid phases, respectively; and $r_{s,m}$. and $r_{s,im}$ are zero-order production terms for the mobile and immobile adsorbed phases, respectively.

3. Experiments

3.1. Rock

The granite, clay rock, and mudstone utilized in this study were sourced from radioactive waste disposal sites under construction, planned construction, and existing sites in northwest, northern, and southwestern China, respectively. Following retrieval, all the rock samples were crushed, washed thrice with deionized water, and dried at 100 ± 10 °C for 24 h before being stored. Both batch and column experiments were conducted. Batch experiments and diffusion experiments were conducted using rock samples with a particle size of 0.075 mm or less. In the column experiment, the particle size of the granite was less than 0.075 mm, while the particle size of the clay rock and mudstone shale ranged from 0.425 mm to 0.25 mm.

3.2. Rock Sample Analysis

X-ray Powder diffractometer (XRD,D-Power, Anhui Guoke Instrument Technology Co., Ltd., Hefei, China), X-ray Fluorescence Spectrometer (XRF, Zetium, Malvern Panalytical, Malvern, UK), and Scanning Electron Microscopy–Energy-Dispersive Spectrometer (SEM-EDS,TH-F120, CIQTEK Co., Ltd., Hefei, China) were utilized to analyze the mineral and chemical composition of the granite, clay rock, and mudstone shale, respectively.

3.3. Batch Experiment

The adsorption behavior was investigated using a batch experiment method. A 1.0 g treated rock sample was weighed and placed in a 15 mL centrifuge tube. Subsequently, a 10 mL nuclide solution (initial activity concentrations of 800 Bq, 1600 Bq, 2400 Bq, 3200 Bq, 4000 Bq) mixed with ultrapure water was added, maintaining a solid–liquid ratio of 1:10 g/mL and a pH value of 7.3–8.0. The mixture was shaken continuously at 25 °C for 48 h to ensure full contact of the sample. Following this, a centrifuge was used to separate the solid and liquid phases. The water sample was then extracted to measure the nuclide's activity and calculate the activity concentration. The ^{99}Tc sample (China Tongfu Co., Ltd., Nantong, China) was analyzed and measured using an ultra-low background liquid scintillation spectrometer (SIM-MAX LSA3000, Shanghai Xinman Sensing Technology Research and Development Co., Ltd., Shanghai, China).

3.4. Diffusion Experiment

3.4.1. Diffusion Experimental Device

Figure 1 illustrates the equipment utilized in the diffusion experiment, comprising three main components: the source liquid tank, the liquid collection tank, and the rock slice. Introduce nuclides into the source liquid tank, fill the liquid tank with ultrapure water devoid of solutes, secure the rock sheet using a porous filter, and position it at the center of the diffusion device using two "O" rings. Additionally, to maintain the long-term integrity of the sample medium and prevent damage, secure the sample with two polyethylene filters on both sides and insert it into the experimental apparatus. The experimental setup parameters are detailed in Table 1.

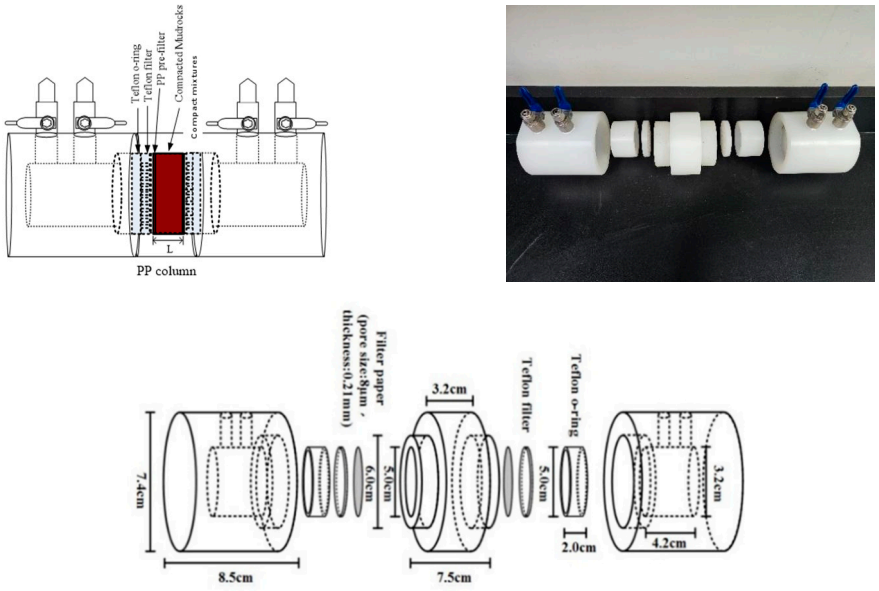


Figure 1. Diffusion experimental device.

Table 1. Diffusion experimental device parameters.

Device	Length (cm)	Diameter (cm)
Diffusion device	20.2 cm	7.4 cm
Source liquid tank (liquid collection tank)	4.2 cm	3.2 cm
rock slice	0.3 cm	5 cm

3.4.2. Diffusion Experimental Procedure

a. Granite, clay rock, and mudstone with a particle size less than 0.075 mm are compacted to obtain experimental samples with a density of 2.0 g/cm^3, and fixed through filters before being placed in a diffusion tank.

b. Water saturation treatment is performed on rock fragments by filling the source liquid tank with ultrapure water. The water is allowed to permeate into the extraction tank under the influence of a water level difference, saturating the rock fragments with water.

c. After saturating the rock fragments with water, the nuclide HTO (20 Bq/mL) is initially introduced into the source liquid tank. This tank is linked to an external storage tank via a peristaltic pump (30–60 min per cycle, with a water flow rate of 500–1000 mL). The solubility of nuclides in the source liquid tank is maintained at a constant level by continuously monitoring the HTO content in the storage tank. Simultaneously, ultrapure water is added to the extraction tank to ensure a consistent water level on both sides. Periodically, all the solutions in the extraction tank are extracted for HTO activity measurement. The diffusion experiment of HTO is concluded once analysis and calculations confirm the attainment of equilibrium. An ultra-low background liquid scintillation spectrometer (SIM-MAX LSA3000, Shanghai Xinman Sensing Technology Research and Development Co., Ltd.) is employed for the analysis and quantification of HTO (China Tongfu Co., Ltd.).

d. After rinsing the HTO clean, the ^{99}Tc (15 Bq/mL) solution is placed into the source tank and connected to an external storage tank using a peristaltic pump (30–60 min per cycle, with a water flow rate of 500–1000 mL). The ^{99}Tc content in the storage tank is continuously measured to ensure constant solubility of nuclides in the source tank. All the solutions are regularly taken out from the tank, and the activity of nuclides is measured. After confirming diffusion equilibrium through analysis and calculation, all diffusion tests are stopped.

3.5. Column Experiment

3.5.1. Column Experimental Device

The device is shown in Figure 2 and consists of three parts: the injection end, column, and collection end. The injection end includes bottle 1 (for storing nuclide solution) and bottle 2 (for storing ultrapure water). The injection of nuclides is achieved by controlling a three-way valve connected to a peristaltic pump. The column is filled with rock and soil samples, and filters are installed at the upper and lower ends to prevent sample loss. The collection end is used for collecting the effluent from the column, and the automatic collector completes the sample sampling at regular intervals. The device parameters are shown in Table 2.

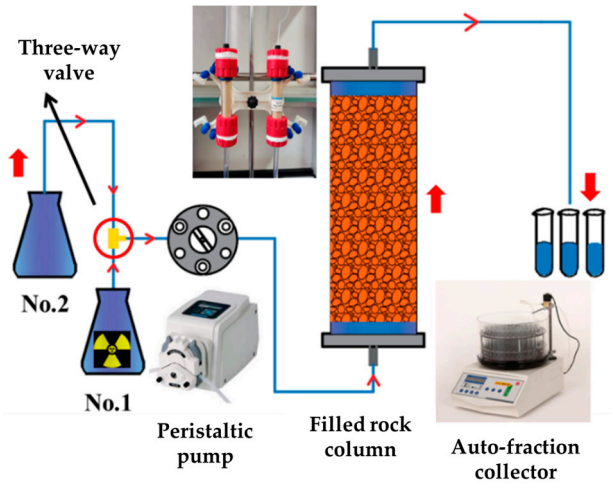


Figure 2. Column experimental device.

Table 2. Column experimental device parameters.

Device	Length	Diameter
Granite column (Particle size < 0.075 mm)	10 cm	1.6 cm
Clay rock column (0.425–0.25 mm)	10 cm	1.6 cm
Mudstone shale column (0.425–0.25 mm)	10 cm	1.6 cm

3.5.2. Column Experimental Procedure

a. Fill the processed granite, clay rock, and mudstone samples into glass columns with a density of 1.25 g/cm^3. Install filter screens at the upper and lower ends of the column to prevent the loss of soil samples during water flow erosion.

b. To saturate the rock column with water, adjust the three-way valve and open the peristaltic pump to slowly inject ultrapure water from the bottom of the column in bottle 2. Stop when water flows out from the outlet to fully saturate the rock and soil column.

c. Inject HTO solution into bottle 1, adjust the three-way valve, and open the peristaltic pump to inject HTO (5000 Bq) into the soil column instantly. Then, regulate the three-way valve to introduce ultrapure water into the column at a flow rate of 0.25 mL/min while keeping the pH within the range of 7.3–8.0. Periodically collect and analyze samples at the outflow end. Cease the HTO penetration test once the HTO content in the outflow falls below the lower limit of detection.

d. After rinsing the HTO in bottle 1, replace it with ^{99}Tc solution and inject ^{99}Tc (5000 Bq) into the soil column instantly following the same steps. Collect samples at the outflow end and analyze them periodically. Terminate the test when the nuclide content in the outflow is below the detection lower limit.

3.6. Mathematical Model and Parameter Estimations

Use 1stOpt 6.0 (First Optimization) software and STANMOD 2.10 (STudio of ANalytic MODels), respectively, to fit the experimental data obtained from diffusion experiments and convection–dispersion experiments. 1stOpt is a comprehensive mathematical optimization analysis tool software package that has achieved good results in handling nonlinear regression, curve fitting, and other problems through the use of the Universal Global Optimization (UGO) algorithm. STANMOD is a Windows-based computer software package used to evaluate solute transport in porous media using analytical solutions of

the advection–dispersion solute transport equation. The software includes modified and updated versions of the CXTFIT code for estimating solute transport parameters using nonlinear least squares parameter optimization methods. Both software use root mean square error (RMSE) to represent the degree of fitting, which is defined as follows:

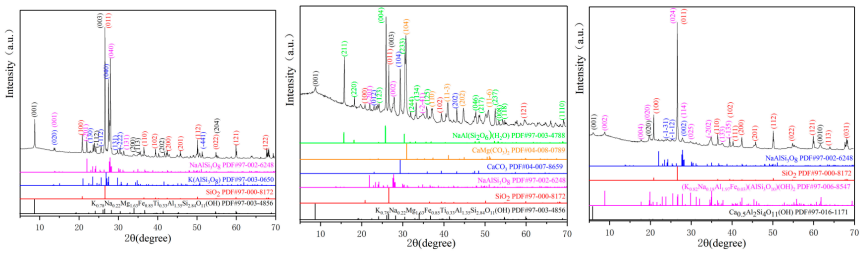
$$RMSE = \sqrt{\frac{\sum_i^N (C_p - C_e)^2}{N}} \quad (12)$$

where C_p denotes the results of the numerical fitting and C_e denotes the experimental data.

4. Results and Discussion

4.1. Mineral Composition and Chemical Composition

The mineral and chemical composition analysis of the granite, clay rock, and mudstone shale is depicted in Figures 3 and 4, and Table 3.



(**a**) Granite (**b**) Clay rock (**c**) Mudstone shale

Figure 3. XRD analysis results of rock samples.

Table 3. Mineral composition and chemical analysis results of rock samples (%).

Rock	Mica	Quartz	Potassium Feldspar	Plagioclase	Illite	Montmorillonite	Zeolite
Granite	10.8	20.5	30.2	38.5	/	/	/
Clay rock	11.1	4.0	/	16.9	/	/	23.6
Mudstone shale	/	46.7	/	9.7	24.6	19.0	/
Rock	Calcite	Dolomite	SiO_2	Al_2O_3	Na_2O	K_2O	CaO
Granite	/	/	66.81	15.88	3.83	4.82	3.43
Clay rock	9.6	34.8	30.61	9.72	3.08	2.14	27.95
Mudstone shale	/	/	61.15	20.81	0.33	5.15	0.67
Rock	Fe_2O_3	MgO	TiO_2	P_2O_5	SO_3	MnO	SrO
Granite	3.04	1.24	0.469	0.146	0.10	0.05	0.05
Clay rock	6.74	14.72	0.621	0.080	3.74	0.20	0.27
Mudstone shale	8.47	2.14	0.88	0.16	0.03	0.08	0.01
Rock	BaO	Rb_2O	ZrO_2	ZnO	La_2O_3	V_2O_5	Cr_2O_3
Granite	0.05	0.02	0.01	0.01	0.01	0.01	0.004
Clay rock	/	0.02	0.02	0.01	/	0.02	0.021
Mudstone shale	0.02	0.03	0.03	/	0.01	0.02	0.020
Rock	Ga_2O_3	PbO	Co_3O_4	Cl	CeO_2	CuO	Er_2O_3
Granite	0.003	0.003	0.002	0.032	/	/	/
Clay rock	0.002	/	0.003	0.083	0.006	0.005	0.004
Mudstone shale	0.003	/	0.003	0.023	/	/	/

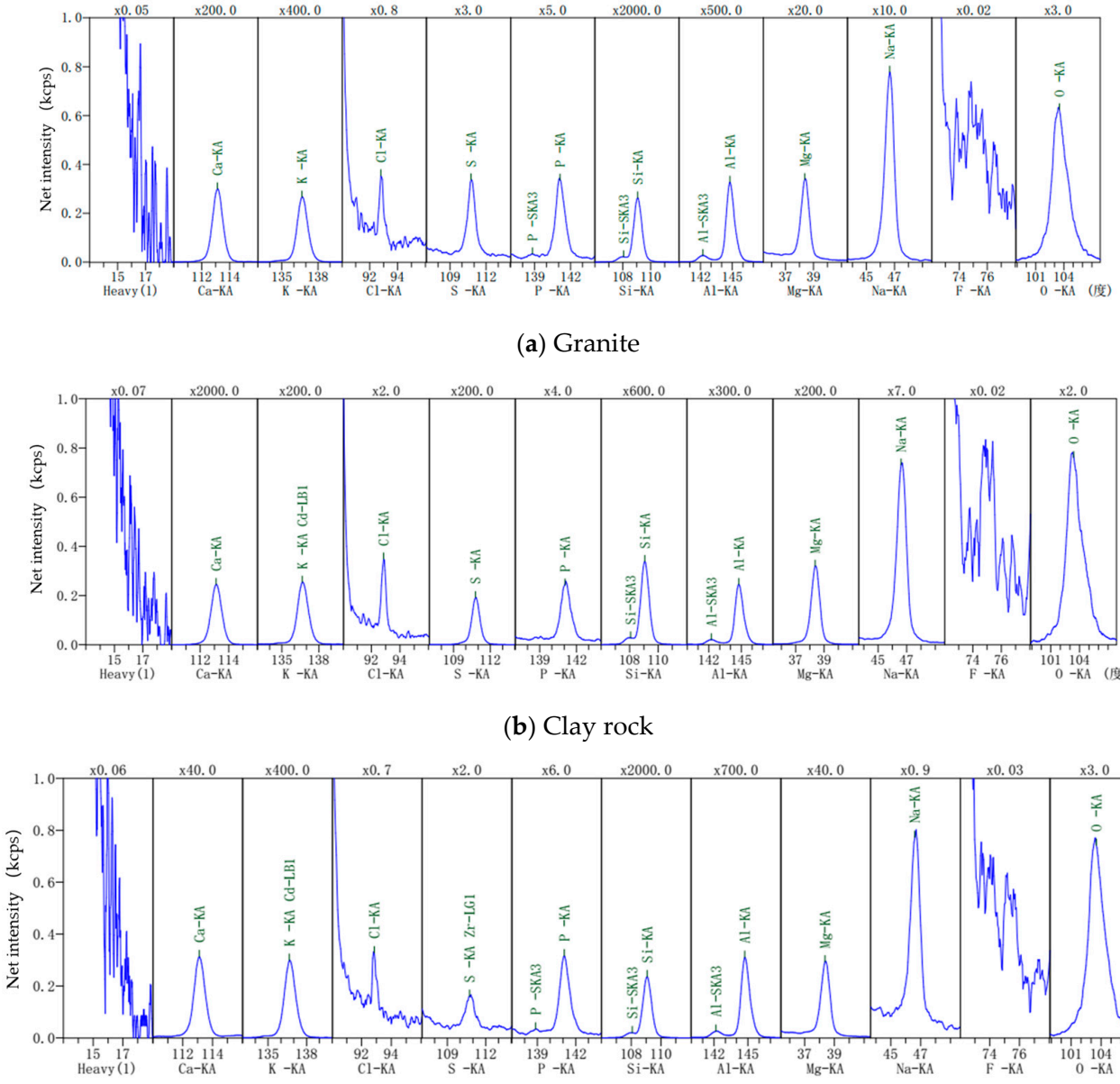


Figure 4. XRF analysis results of rock samples.

4.2. Batch Experiment Results

Batch experiments were carried out to investigate the adsorption behavior of ^{99}Tc in the granite, clay rock, and mudstone shale. The results are illustrated in Figure 5. The distribution coefficients of ^{99}Tc for the granite, clay rock, and mudstone shale are 0.85 mL/g, 0.78 mL/g, and 0.30 mL/g, respectively. The solid-phase adsorption capacity in this study was determined by subtracting the liquid phase content post-adsorption from the total input amount, considering measurement errors in the liquid phase sample and solute losses during operations. Subsequent diffusion and convection–dispersion experiments indicated that the granite, clay rock, and mudstone shale exhibited negligible adsorption capacity for ^{99}Tc in this investigation.

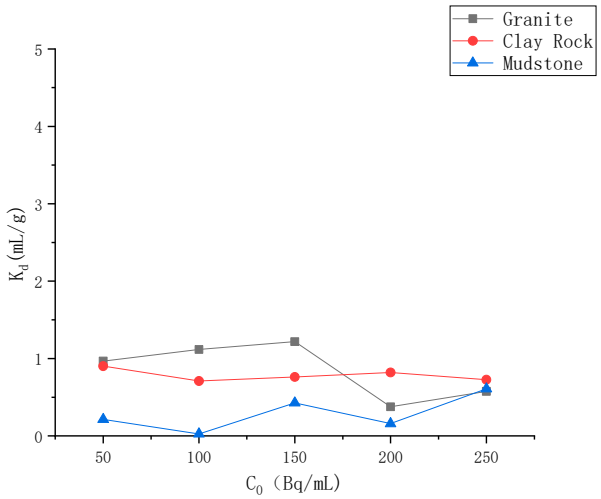
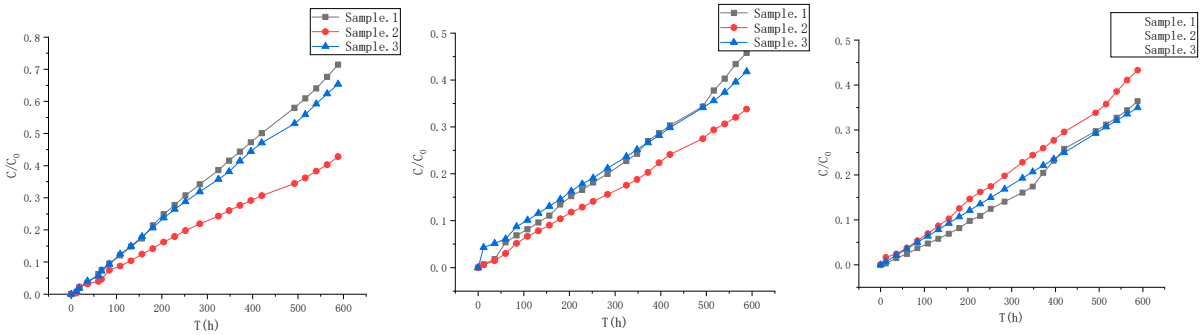


Figure 5. Adsorption capacity of different rocks for ^{99}Tc.

4.3. Diffusion Experiment Results

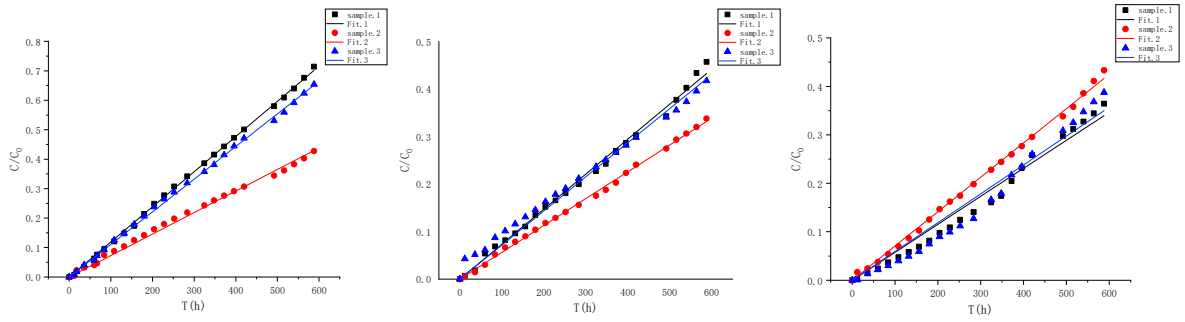
4.3.1. Diffusion Experiment Results of HTO

To examine the diffusion pathways within the granite, clay rock, and mudstone shale, experiments were conducted to analyze the diffusion characteristics of tritiated water (HTO) within them. The experimental findings are shown in Figure 6. Each material was tested in triplicate, with each test lasting 588 h. Following the initiation of the experiments, the diffusion profiles of HTO in all the substrates exhibited a swift escalation. The diffusion capacity of HTO in the three rock types follows the order granite > clay rock > mudstone shale. The diffusion parameters were determined through numerical simulation methods, and the fitting effect, along with related parameters, is presented in Figure 7 and Table 4. The experimental results demonstrate variations in porosity among different rock types: granite (Ø = 0.26) > mudstone shale (Ø = 0.20) > claystone (Ø = 0.18). Regarding the effective diffusion coefficient, a notable discrepancy exists within the granite samples, with values ranging from 2.48×10^{-12} to 4.05×10^{-11} m^2/s. In contrast, the disparity between clay rock and mudstone shale is insignificant, with diffusion coefficients ranging from 2.60×10^{-11} to 1.99×10^{-11} m^2/s and 2.03×10^{-11} to 2.50×10^{-11} m^2/s, respectively.



(**a**) Granite (**b**) Clay rock (**c**) Mudstone shale

Figure 6. Diffusion curves of HTO in different rocks.



(**a**) Granite (**b**) Clay rock (**c**) Mudstone shale

Figure 7. Fitting of diffusion curves of HTO in different rock media.

Table 4. Parameters for fitting diffusion curves of HTO in different rock media.

Rock	Ø	α	D_a	D_e	R^2	RMSE
Granite-1	0.26	0.26	1.56×10^{-10} m^2/s	4.05×10^{-11} m^2/s	0.999	0.060
Granite-2	0.26	0.26	9.54×10^{-11} m^2/s	2.48×10^{-12} m^2/s	0.998	0.094
Granite-3	0.26	0.26	1.45×10^{-10} m^2/s	3.76×10^{-11} m^2/s	0.999	0.067
Clay rock-1	0.18	0.18	1.42×10^{-10} m^2/s	2.60×10^{-11} m^2/s	0.998	0.096
Clay rock-2	0.18	0.18	1.09×10^{-10} m^2/s	1.99×10^{-11} m^2/s	0.999	0.042
Clay rock-3	0.18	0.18	1.38×10^{-10} m^2/s	2.53×10^{-11} m^2/s	0.998	0.161
Mudstone shale-1	0.20	0.20	1.02×10^{-10} m^2/s	2.03×10^{-11} m^2/s	0.994	0.172
Mudstone shale-2	0.20	0.20	1.25×10^{-10} m^2/s	2.50×10^{-11} m^2/s	0.999	0.063
Mudstone shale-3	0.20	0.20	1.05×10^{-10} m^2/s	2.10×10^{-11} m^2/s	0.989	0.260

4.3.2. Diffusion Experiment of ^{99}Tc

The ^{99}Tc diffusion curve is depicted in Figure 8. Generally, the diffusion pattern of ^{99}Tc resembles that of HTO, suggesting negligible adsorption impact of the medium on ^{99}Tc.

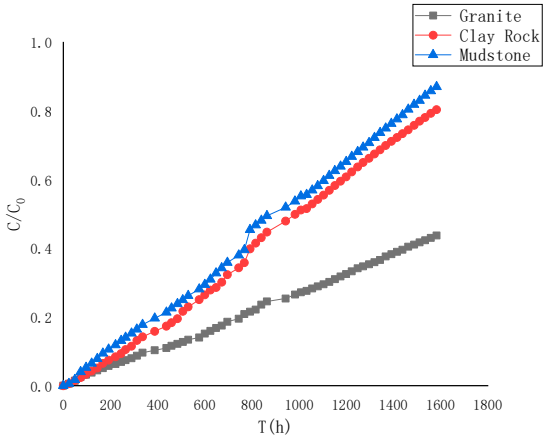


Figure 8. Diffusion curves of ^{99}Tc in different rocks.

The diffusion experiment lasted for 1584 h, and the cumulative concentration ratio of ^{99}Tc in different rock media was granite < clay rock < mudstone shale, which contrasts significantly with the diffusion behavior of HTO. This difference is attributed to ^{99}Tc existing in an anionic state (TcO_4^-) in aqueous solution, leading to repulsion by anions in the rock pores. This repulsion results in the blockage of small pores while accelerating the migration

of nuclides in larger pores. Moreover, a higher clay mineral content intensifies the repulsive effect, indicating that ^{99}Tc diffuses most rapidly in mudstone shale and slowest in granite.

For the fitting of the diffusion curve of ^{99}Tc, the "anion repulsion" effect, not explicitly defined in current diffusion models, influences both the distribution coefficient (represented by negative values) and the effective diffusion coefficient (leading to a significant decrease). These parameters directly impact the capacity factor α and porosity $\emptyset$ in the fitting process. To enhance the precision of the fitting parameters, the primary approach involves initially determining the apparent diffusion coefficient *Da* and capacity factor α through curve fitting. Subsequently, the effective diffusion coefficient *De* is calculated, with the fixed porosity $\emptyset$ remaining constant at its original value and the distribution coefficient set at 0. This method consolidates all the anion repulsion effects within the effective diffusion coefficient.

The results of the fitting are displayed in Figure 9 and Table 5. Upon comparing the parameters across various rock types, it was observed that the apparent diffusion coefficient follows the order: mudstone > clay rock > granite. Similarly, the order for mud shale > clay rock > granite remains consistent. Regarding the effective diffusion coefficient, the sequence mudstone shale > clay rock > granite was noted, suggesting that the "anion repulsion" of ^{99}Tc leads to an overall "accelerated" diffusion of nuclides. Notably, a stronger "anion repulsion" corresponds to a smaller effective diffusion coefficient in these parameters.

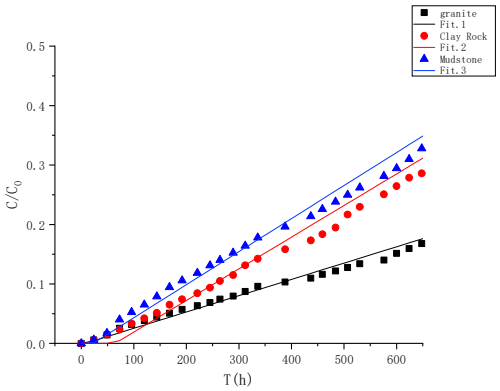


Figure 9. Fitting of diffusion curves of ^{99}Tc in different rock media.

Table 5. Parameters for fitting diffusion curves of ^{99}Tc in different rock media.

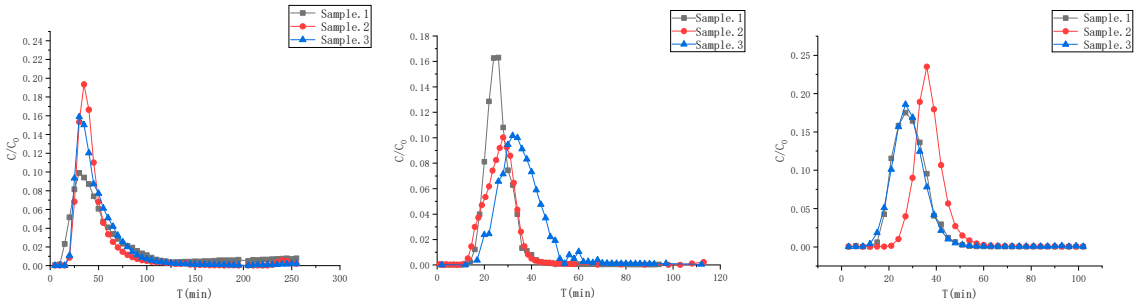
Rock	$\emptyset$	α	D_a (m^2/s)	D_e (m^2/s)	K_d (mL/g)	R^2	*RMSE*
Granite	0.26	0.26	3.59×10^{-11}	9.34×10^{-12}	0	0.999	0.006
Clay rock	0.18	0.18	8.97×10^{-11}	1.71×10^{-11}	0	0.998	0.014
Mudstone shale	0.20	0.20	9.28×10^{-11}	1.86×10^{-11}	0	0.997	0.014

4.4. Advection–Dispersion Experiment of ^{99}Tc

4.4.1. Advection–Dispersion Experiment Results of HTO

The experimental results are depicted in Figure 10. Overall, the advection–dispersion migration curves of HTO in different rocks exhibit an "S" shape, consistent with the advection–dispersion curve under the instantaneous input mode of non-adsorbed solutes in homogeneous media. To ensure future accuracy in determining relevant physical migration parameters of the medium, three parallel samples are analyzed for each case. The HTO experiment in granite columns lasted 255 min, with peak occurrences at 30, 35, and 30 min, and corresponding peak values of 0.094, 0.193, and 0.159, respectively. For clay rock columns, the experimental durations were 96 min, 103 min, and 97 min, with peak

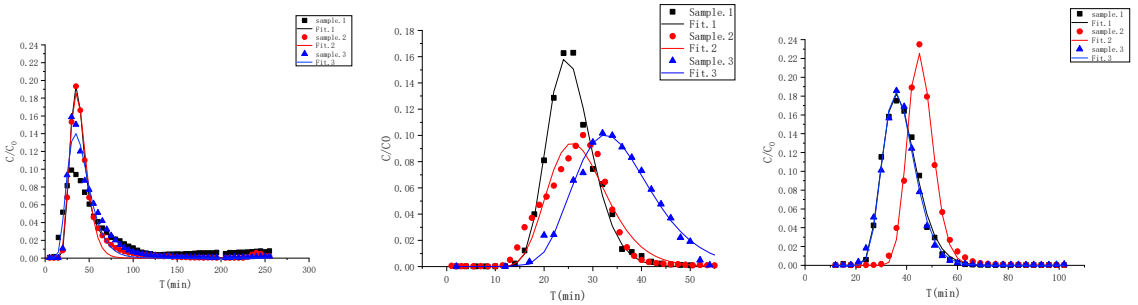
values observed at 24, 28, and 32 min, with corresponding peak values of 0.163, 0.100, and 0.100, respectively. In shale columns, the experimental duration of HTO was 102 min, with peak values recorded at 27, 36, and 27 min, with corresponding peak values of 0.175, 0.235, and 0.190, respectively.



(**a**) Granite (**b**) Clay rock (**c**) Mudstone shale

Figure 10. Advection–dispersion curves of HTO in different rocks.

The advection–dispersion parameters were determined through a balanced model fitting. The fitting effect and associated parameters are presented in Figure 11 and Table 6, respectively. The dispersion values for granite range from 0.631 to 0.640 cm, for clay rock from 0.248 to 0.285 cm, and for mudstone from 0.263 to 0.323 cm.



(**a**) Granite (**b**) Clay rock (**c**) Mudstone shale

Figure 11. Fitting of advection–dispersion curves of HTO in different rock media.

Table 6. Parameters for fitting advection–dispersion curves of HTO in different rock media.

Rock	*V*	*D*	D_L	*R*	*RMSE*
Granite-1	0.241 cm/min	0.152 cm^2/min	0.631 cm	1.00	5.25×10^{-6}
Granite-2	0.242 cm/min	0.155 cm^2/min	0.640 cm	1.00	3.89×10^{-6}
Granite-3	0.242 cm/min	0.154 cm^2/min	0.636 cm	1.00	9.45×10^{-5}
Clay rock-1	0.383 cm/min	0.095 cm^2/min	0.248 cm	1.00	1.57×10^{-5}
Clay rock-2	0.358 cm/min	0.095 cm^2/min	0.269 cm	1.00	3.46×10^{-10}
Clay rock-3	0.322 cm/min	0.092 cm^2/min	0.285 cm	1.00	9.26×10^{-6}
Mudstone shale-1	0.342 cm/min	0.098 cm^2/min	0.287 cm	1.00	1.04×10^{-5}
Mudstone shale-2	0.312 cm/min	0.101 cm^2/min	0.323 cm	1.00	1.24×10^{-5}
Mudstone shale-3	0.346 cm/min	0.091 cm^2/min	0.263 cm	1.00	9.14×10^{-6}

4.4.2. Advection–Dispersion Experiment Results of ^{99}Tc

The advection–dispersion behavior of ^{99}Tc in the granite, clay rock, and mudstone shale is illustrated in Figure 12. The migration curve of ^{99}Tc in granite and clay rock exhibits an "S" shape, while the migration curve of mudstone shows a distinct "tailing" phenomenon. This observation is attributed to the "anion repulsion" of ^{99}Tc during the convection–dispersion process in mudstone. This phenomenon causes a more pronounced

"blockage" of small pores in mudstone compared to granite and clay rock, leading to delayed outflow of certain nuclides and the emergence of a "tailing" effect.

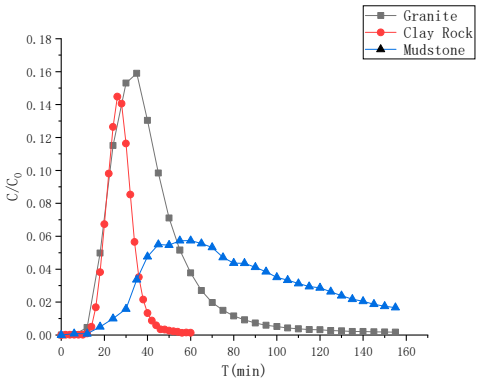
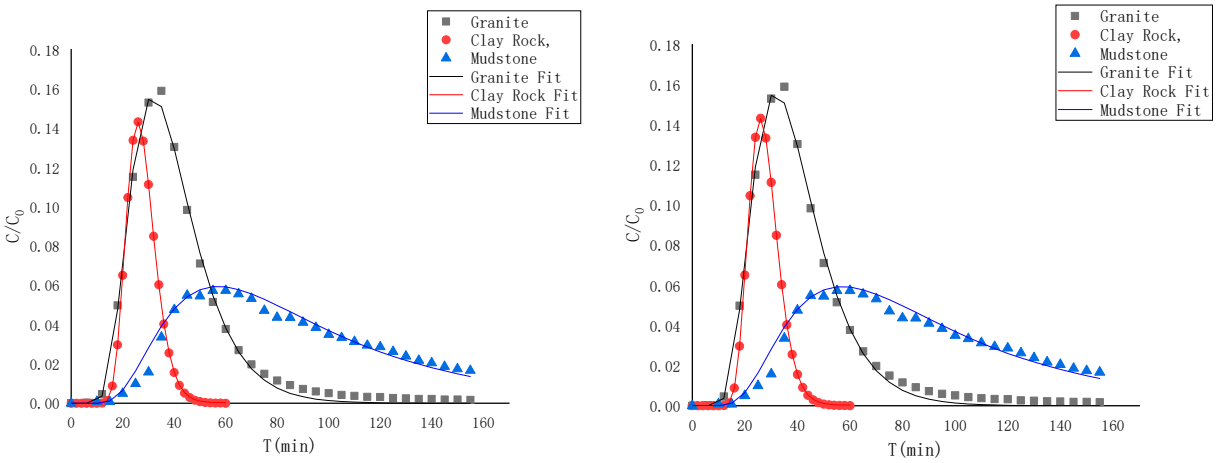


Figure 12. Advection–dispersion curves of ^{99}Tc in different rocks.

Different numerical models were utilized to fit the ^{99}Tc advection–dispersion migration curves in granite, clay rock, and mudstone shale. The fitting outcomes and associated parameters are presented in Figure 13 and Table 7. Initially, the equilibrium transport (E-T) model was applied to fit the advection–dispersion migration curves of ^{99}Tc in various rocks, demonstrating a satisfactory fitting effect. However, the calculated distribution coefficients were consistently negative, which contradicted the actual conditions. This discrepancy suggests that ^{99}Tc experiences "anion repulsion" during migration, leading to some channels being "blocked", resulting in negative distribution coefficients derived from the equilibrium transport model. Subsequently, the two-region nonequilibrium transport (T-N) model was employed to fit the curves and derive the relevant transfer parameters. The dispersion, movable zone porosity, and immovable zone porosity of ^{99}Tc in granite migration are 0.630 cm, 0.26 cm, and 0.11 cm, respectively; in clay rock, they are 0.215 cm, 0.16 cm, and 0.15 cm, respectively; and in mudstone, they are 0.320 cm, 0.17 cm, and 0.18 cm, respectively. Comparing the immovable zone porosity proportions, it was observed that the "anion repulsion" effect influences the ^{99}Tc migration behavior in mudstone in the following order: (51%) > clay rock (48%) > granite (30%).



(**a**) E-T model (**b**) T-N model

Figure 13. Fitting of advection–dispersion curves of ^{99}Tc in different rock media.

Table 7. Parameters for fitting advection–dispersion curves of ^{99}Tc in different rock media.

Model			**Granite Column**			
E-T	V 0.254 cm/min	D 0.16 cm^2/min	D_L 0.630 cm	R 0.981	K_d <0	RMSE 1.97×10^{-5}
T-N	V 0.254 cm/min	D 0.16 cm^2/min	D_L 0.630 cm	θ_m 0.26	θ_{im} 0.11	RMSE 1.10×10^{-5}
Model			Clay rock column			
E-T	V 0.256 cm/min	D 0.055 cm^2/min	D_L 0.215 cm	R 0.707	K_d <0	RMSE 1.60×10^{-5}
T-N	V 0.256 cm/min	D 0.055 cm^2/min	D_L 0.215 cm	θ_m 0.16	θ_{im} 0.15	RMSE 1.45×10^{-5}
Model			Mudstone shale column			
E-T	V 0.286 cm/min	D 0.092 cm^2/min	D_L 0.320 cm	R 0.954	K_d <0	RMSE 1.14×10^{-5}
T-N	V 0.286 cm/min	D 0.092 cm^2/min	D_L 0.320 cm	θ_m 0.17	θ_{im} 0.18	RMSE 1.07×10^{-5}

5. Conclusions

A systematic study was conducted on the adsorption, diffusion, and advection–dispersion behavior of ^{99}Tc in granite, clay rock, and mudstone shale, with a focus on the influence of "anion repulsion" on the migration process of ^{99}Tc. The key parameters were obtained through numerical fitting to quantify their degree of influence. The research conclusions are as follows:

1. Batch experiments were conducted, revealing that granite, clay rock, and mudstone shale exhibited negligible adsorption of ^{99}Tc.

2. The anion exclusion observed in the diffusion of ^{99}Tc can impede certain narrow channels, demonstrating that a higher anion exclusion leads to a reduced effective diffusion coefficient. Conversely, the anion exclusion can enhance the diffusion rate of ^{99}Tc in wider water channels. Moreover, the anion exclusion encountered during the diffusion of ^{99}Tc is more pronounced in shale than in clay or granite.

3. ^{99}Tc is influenced by anion exclusion in the advection–dispersion process, making it challenging to achieve satisfactory fitting results using the equilibrium transport model. Therefore, employing a two-region nonequilibrium transport model becomes essential to accurately determine parameters such as porosity in the immobile zone due to anion exclusion across various media.

Author Contributions: Conceptualization, Y.S. and A.Z.; methodology, Y.S. and S.Y.; software, Y.S. and W.C.; validation, Y.S. and B.L.; formal analysis, Y.S. and Z.L.; investigation, A.Z. and S.Y.; resources, B.L. and L.W.; data curation, Y.S. and W.C.; writing—original draft preparation, Y.S. and S.Y.; writing—review and editing, Y.S. and Z.L.; visualization, Y.S. and S.Y.; supervision, L.W. and B.L.; project administration, Y.S. and B.L.; funding acquisition, Z.L. and B.L. All authors have read and agreed to the published version of the manuscript.

Funding: This project was mainly supported by the "Study on the Mechanism and Model of Multi-nuclide Transport in Granite Fracture under Competitive Adsorption". (No. 42402242), Natural Science Foundation of China, Shanxi Province Basic Research Project (No. SN22010301), and Start-up funds for doctoral research of East China University of Technology (No. 1410000434).

Institutional Review Board Statement: Not applicable for studies not involving humans or animals.

Informed Consent Statement: Not applicable.

Data Availability Statement: The raw data supporting the conclusions of this article wil be made available by the authors on request.

Acknowledgments: The experimentation conducted in this study was assisted by Chuan-Pin Lee, members of the Chemistry and Analysis Division of the Institute of Nuclear Energy Research, Taiwan. Assistance in conducting the experimental and instrumental analyses of this study was provided by the East China University of Technology, Nanchang, Jiangxi, China.

Conflicts of Interest: The authors declare no conflicts of interest.

References

1. IAEA. *IAEA Safety Standards Series No. GSG-1: Classification of Radioactive Waste*; IAEA: Vienna, Austria, 2009.
2. Sharif, A.D.; Hossam, A.G.; Vahid, D. A Comprehensive Review on Radioactive Waste Cycle from Generation to Disposal. *J. Radioanal. Nucl. Chem.* **2021**, *329*, 15–31.
3. Bruno, J.; Delos, A. *Safety Assessment of Nuclear Waste Repositories: A Radionuclide Migration Perspective*; A volume in Woodhead Publishing Series in Energy; Woodhead Publishing: Cambridge, UK, 2012; pp. 646–692.
4. Wang, X.; Liu, C.; Wang, C.; Li, C.; Chen, T. Adsorption and Diffusion of Some Important Radionuclides in Beishan Granites and Gaomiaozi Bentonites. *Sci. Sin. Chim.* **2020**, *50*, 1585–1599. [CrossRef]
5. Daniel, R. Sorption of Neptunium on Clays and Clay Minerals—A Review. *Clays Clay Miner.* **2015**, *64*, 262–276.
6. Marsily, G.D.; Julio, G.; Sophie, V. Migration mechanisms of radionuclides from a clay repository toward adjacent aquifers and the surfaceMécanismes de migration des radionucléides d'un stockage de déchets radioactifs dans l'argile vers la surface. *Comptes Rendus Phys.* **2002**, *3*, 945–959. [CrossRef]
7. IAEA. *Handbook of Parameter Values for the Prediction of Radionuclide Transfer in Terrestrial and Freshwater Environments*; IAEA: Vienna, Austria, 2010.
8. Lee, C.P.; Hu, Y.Q.; Tien, N.C.; Tsai, S.-C.; Shi, Y.; Liu, W.; Kong, J.; Sun, Y. Molecule Diffusion Behavior of Tritium and Selenium in Mongolia Clay Rock by Numerical Analysis of the Spatial and Temporal Variation. *Minerals* **2021**, *11*, 875. [CrossRef]
9. Sun, Y.Z. Study on the Adsorption and Diffusion of Nuclide ^{79}Se(IV)/^{79}Se(IV) in Tamusu Clay Rock. *East China University of Technology* **2023**.
10. Qi, L.L. The Sorption and Transport of Se(IV) and Sr(II) in Granite and the Impact Mechanism of Fracture Filling Materials. 2023.
11. Wang, K.; Zhang, R.D. Heterogeneous Soil Water Flow and Macropores Described with Combined Tracers of Dye and Iodine. *J. Hydrol.* **2011**, *397*, 105–117. [CrossRef]
12. Zaheer, M.; Zhang, W.; Zhan, H.B. An Experimental Study on Solute Transport in One-Dimensional Clay Soil Columns. *Geofluids.* **2017**, *2017*, 6390607. [CrossRef]
13. McCarter, C.P.R.; Rezanezhad, F.; Gharedaghloo, B. Transport of Chloride and Deuterated Water in Peat: The Role of Anion Exclusion, Diffusion, and Anion Adsorption in A Dual Porosity Organic Media. *J. Contam. Hydrol.* **2019**, *225*, 103497. [CrossRef]
14. Mäder, U. Advective Displacement Method for the Characterisation of Pore Water Chemistry and Transport Properties in Claystone. *Geofluids* **2018**, *2018*, 8198762. [CrossRef]
15. Van Loon, L.R.; Soler, J.M.; Jakob, A. Effect of Confining Pressure on the Diffusion of HTO, $^{36}Cl^-$ and $^{125}I^-$ in A Layered Argillaceous Rock (Opalinus Clay): Diffusion Perpendicular to the Fabric. *Geochem* **2003**, *18*, 1653–1662. [CrossRef]
16. Shi, Y.F.; Yang, S.; Chen, W.J. Study on Tritium and Iodine Species Transport Through Porous Granite: A Non-Sorption Effect by Anion Exclusion. *Toxics* **2022**, *10*, 540. [CrossRef]
17. Steigman, J.; Meinken, G.; Richards, P. The Reduction of Pertechnetate-99 by stannous Chloride-II. The Stoichiometry of the Reaction in Aqueous Solutions of Several Phosphorus(V) Compounds. *Int. J. Appl. Radiat. Isot.* **1978**, *29*, 653–660. [CrossRef]
18. He, A.D.; Fu, Z.H.; Yin, Z. The Coordination of Low-valent Re/Tc with Glutarimide Dioxime and the Fate of Tc in Aqueous Solution: Spectroscopy, ESI-MS and EXAFS. *J. Radioanal. Nucl. Chem.* **2021**, *328*, 1279–1289. [CrossRef]
19. Sheng, G.D.; Guo, Z.Q.; Yang, S.T. Application of XAFS Technique in Interface Interaction Study of Radionuclides in Environment. *Prog. Chem.* **2011**, *23*, 1455–1468.
20. Liu, C.L.; Wang, X.Y.; Gao, H.C. Diffusion Behavior of Some Weakly Absorbed Nuclide Species in Granite. *J. Nucl. Radiochem.* **2003**, *25*, 204–209.
21. Lee, C.P.; Hu, Y.Q.; Chen, D.Y. A Statistical Evaluation to Compare and Analyze Estimations of the Diffusion Coefficient of Pertechnetate ($^{99}TcO_4^-$) in Compacted Bentonite. *Minerals* **2021**, *11*, 1075. [CrossRef]
22. Tsai, T.L.; Tsai, S.C.; Shih, Y.H. Diffusion Characteristics of HTO and $^{99}TcO_4^-$ in Compacted Gaomiaozi (GMZ) Bentonite. *Nucl. Sci. Tech.* **2017**, *28*, 67. [CrossRef]
23. Poinssot, C.; Geckeis, H. *Radionuclide Behaviour in the Natural Environment. Implications and Lessons for the Nuclear Industry*; Woodhead Publishing: Cambridge, UK, 2012.

24. Šimůnek, J.; Šejna, M.; Sait, H. *The HYDRUS-1D Software Package for Simulating the One-Dimensional Movement of Water, Heat, and Multiple Solutes in Variably-Saturated Media*; Department of Environmental Sciences University of California Riverside Riverside: Riverside, CA, USA, 2018.
25. Kong, J.; Sun, Y.Z.; Hua, R. Anion Exclusion and Sorption Effect for Compacted Bentonite: The Dependency of Diffusion Coefficients and Capacity of HTO and Se(IV). *J. Radioanal. Nucl. Chem.* **2021**, *4*, 1588–2780. [CrossRef]
26. Shi, Y.F.; Lee, C.P.; Yu, H.Q. Study on Advection-dispersion Behavior for Simulation of HTO and Se Transport in Crushed Granite. *J. Radioanal. Nucl. Chem.* **2021**, *328*, 1329–1338. [CrossRef]
27. *ASTM C1733-17a*; Standard Test Method for Distribution Coefficients of Inorganic Species by the Batch Method. ASTM: West Conshohocken, PA, USA, 2017.
28. Zhang, X.Y.; Ma, F.; Dai, Z.X. Radionuclide Transport in Multi-scale Fractured Rocks: A Review. *J. Hazard. Mater.* **2021**, *424*, 1016. [CrossRef] [PubMed]
29. Shi, Y.F.; Yang, S.; Wu, E.H. Advection-Dispersion Behavior for Simulation of H-3 and Pu-238 Transport in Undisturbed Argillaceous Shale of a Near-Surface Repository. *Toxics* **2023**, *11*, 124. [CrossRef] [PubMed]
30. IAEA. *Generic Models for Use in Assessing the Impact of Discharges of Radioactive Substances to the Environment*; IAEA: Vienna, Austria, 2001.
31. Grathwohl, P. *Diffusion in Natural Porous Media: Contaminant Transport, Sorption/Desorption and Dissolution Kinetics*; Springer Science & Business Media: Berlin/Heidelberg, Germany, 1998.
32. Hemond, H.F.; Fechner, E.J. *Chemical Fate and Transport in the Environment*; Academic Press: New York, NY, USA, 1994.
33. Krupp, H.K.; Biggar, J.W.; Nielsen, D.R. Relative Fow Rates of Salt and Water in Soil. *Soil Sci. Soc. Am. Proc.* **1972**, *36*, 412–417. [CrossRef]

Disclaimer/Publisher's Note: The statements, opinions and data contained in all publications are solely those of the individual author(s) and contributor(s) and not of MDPI and/or the editor(s). MDPI and/or the editor(s) disclaim responsibility for any injury to people or property resulting from any ideas, methods, instructions or products referred to in the content.